A Connectionist Approach to SODAR Pattern Classification

Swati Choudhury and Sushmita Mitra, *Senior Member, IEEE*

***Abstract*—SODAR (or acoustic radar) systems are a useful tool to efficiently probe the lower planetary boundary layer (LPBL). The observations obtained by these systems can prove to be extremely useful if classified and interpreted correctly. The manual identification of different types of SODAR-recorded lower atmospheric microstructures is a laborious task and can be performed only by an expert having wide experience with the system and the variety of observations recorded by it. In this letter, we have developed a connectionist system to classify or identify SODAR patterns. The results demonstrate that the multilayer perceptron-based model is capable of successfully identifying the different SODAR patterns.**

***Index Terms*—Acoustic remote sensing, classification, connectionist models, neural networks, SODAR identification.**

I. Introduction

THE FIRST 10 km of the atmosphere adjacent to the earth's surface is known as the troposphere. Although the average height of the troposphere is 10 km, individually over the pole, temperate latitude and equator the average heights are 6, 11, and 18 km, respectively. Similarly, the first 1 km of the tropospheric environment, adjacent to the earth's surface, is known as the lower planetary boundary layer (LPBL) or planetary boundary layer (PBL). The average height of the LPBL also varies with respect to space and time. Over the ocean, the average height may be only a few hundred meters, and on the plain land covered with green paddy fields and vegetation, it is 1 km approximately, whereas over the desert region it may extend up to 2 km [1], [2].

The LPBL, with its one end remaining in the immediate vicinity of the ground, plays a vital role in the transfer of heat, energy, and momentum from the ground level to higher levels and vice-versa. It plays an active part in the formation of various phenomena such as thunderstorms, cyclones, rains, floods, and hailstorms. Some other events, such as the propagation of radiowaves, accumulation and dispersion of pollutants, and landing and taking-off of aircraft, are solely dependent on the properties of the lower atmospheric environment. Therefore, the need to probe the LPBL has long been realized by meteorologists, climatologists, and scientists working in the areas of wireless communication, civil aviation, and related fields.

Rapid scientific and technological developments around the world, over the past few decades, have resulted in the design of a variety of sensors for the efficient monitoring of the surface to higher levels of the atmosphere on both a continuous and discrete basis. Presently, there exist two basic techniques to explore the atmospheric environment, *viz.* 1) *in situ* or direct measurement and (2) remote sensing. The most commonly used artificial *in situ* techniques are radiosonde, instrumented tower, microwave refractometer, and airborne systems.

Remote sensing techniques are comparatively recent and can be operated around-the-clock without human intervention. This can again be divided into two categories: passive and active. Radiometer, satellite imagery, etc. are examples of passive remote sensing techniques. On the other hand, active measurement involves the transmission and reception of electromagnetic, light, and acoustic energy. The three commonly used detection and ranging systems ("dars") are: 1) radar; 2) Lidar; and 3) SODAR, corresponding to the three types of radiation used [3]–[5].

SODAR (or acoustic radar) plays a very significant role in probing of the LPBL. This is because the interaction of sound waves with the lower atmosphere is stronger as compared to the electromagnetic spectrum [6]. It can be designed at a reasonable cost and is capable of providing the three-dimensional (3-D) (height, time, and intensity) view of the lower atmospheric microstructures, appearing during different time, month, and season, over a particular region [7]–[9].

Recently, data obtained from different types of monostatic and bistatic SODAR systems have been used to facilitate research in a number of areas of atmospheric sciences, microwave propagation, civil aviation, and various other related fields. Atmospheric turbulence has been studied using doppler SODAR [10]. The authors have measured the scattering cross section σ of the acoustic signal and frequency broadening of the scattered signal ΔF on a simultaneous basis and have shown that there exists a high correlation between σ and ΔF^2. Tropospheric scintillation has been investigated at 7.6 GHz over the Tirutani–Tirupati line-of-sight microwave link [11]. The authors could correlate the nighttime scintillations with the SODAR structures.

Potential use of SODAR data can be made, provided it can be interpreted and identified correctly. So far, the task of identification of SODAR-recorded observations has been completely dependent on the knowledge, experience, and expertise of researchers working with the system and its recorded observations for a reasonable period of time. This restricts the utility of the data to a limited number of persons having expertise in the field. Utilization of the full potential of SODAR observations on a global basis calls for the existence of computer-based techniques, developed preferably by incorporating human expertise.

Artificial neural networks (ANNs) or connectionist models [12], [13] attempt to replicate the *computational* power (low-level arithmetic processing ability) of biological neural networks and, thereby, hopefully endow machines with some of the (higher level) *cognitive abilities* that biological organizms possess (due

The authors are with the Machine Intelligence Unit, Indian Statistical Institute, Kolkata 700 108, India (e-mail: swati_v@isical.ac.in; sushmita@isical.ac.in).

in part, perhaps, to their low-level computational prowess). The multilayer perceptron (MLP) is a well-known feed-forward ANN model that is typically used in pattern classification problems. Here, supervised learning is done in the presence of given class labels. The main utility of the network lies in its capability in discovering the inherent relationships existing in the pattern domain. It can be suitably used in data-rich environments.

Atmospheric sciences naturally involve processing of large volumes of data. Efforts have been made to handle the analysis of atmospheric data using some standard statistical and mathematical methods. The Bayes classifier and k-nearest neighbor classifier [14] have been used to distinguish between two classes of SODAR patterns, *viz.*, convective thermal plumes and temperature inversion [15]. An elementary attempt to classify the SODAR data has been made using fractal features [16]. Fractal dimension (FD) has been estimated for few SODAR patterns and it is showed that FD values change from pattern to pattern. Finally, it is inferred that classification can be made on the basis of varying FD values.

MLPs have also been recently applied in this domain of atmospheric sciences. Neural-network-based techniques have been used in the prediction of tornado and damaging wind conditions [17], [18]. A fuzzy MLP has been employed to successfully classify radio-refraction conditions of the tropospheric environment, categorized as subrefraction, normal-refraction, and superrefraction [19]. It holds promise in tropospheric wireless communication, meteorology, and related fields.

The objective of this letter is to design a connectionist decision-making system for the classification of different SODAR images. The proposed system is able to exploit the parallelism, self-learning and fault tolerance characteristics of ANN models. We have used an MLP to classify different types of observations obtained from a 2350-Hz monostatic SODAR system [20]. The results demonstrate effective classification of single-layer SODAR structures in terms of their recognition scores.

Section II provides a brief description of the SODAR system and the types of observations used for the identification. The experimental results, obtained using an MLP with the SODAR data, are provided in Section III. Finally, the letter is concluded in Section IV.

II. SODAR System: Description and Observations

The main objective behind the design and development of a SODAR system was to capture the formation of thermal plumes, various types of inversion layers, etc., that appeared in the LPBL persisting at our site of experiment. Therefore, a 2350-Hz monostatic SODAR system was installed at the Indian Statistical Institute (Kolkata, India). Kolkata (located at 22°N and 88°E) being situated near the eastern coastal region of India, is well affected by land-sea interaction, and the average height of LPBL over this region remains well within the range of 1 km [20].

A simple block diagram of a 2350-Hz SODAR system is shown in Fig. 1. The system has a tunable oscillator with a frequency range of 1–4 KHz. The output (signal of the desired frequency) of this oscillator is fed to a tone burst generator, which generates a pulse of the desired shape and duration. The pulsed signal is amplified in a commercial audio power amplifier (135 W) and transmitted through an acoustic transducer

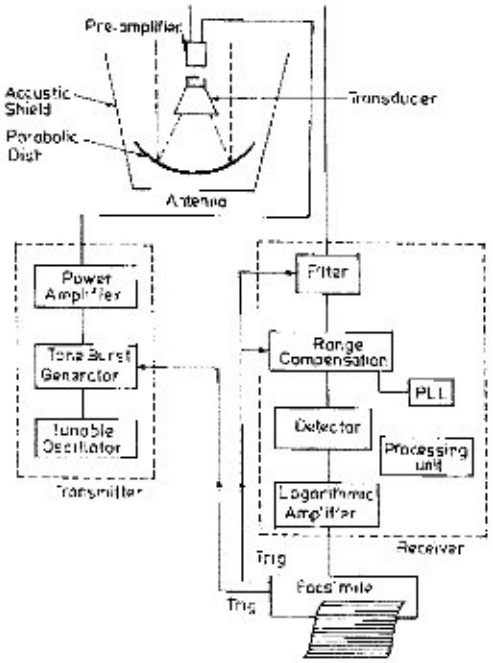

Fig. 1. Simple block diagram of a 2350-Hz monostatic SODAR system.

TABLE I
SODAR System Specification

Transmitting frequency	1 to 4 kHz (tunable)
Pulse width	10 to 100 ms (adjustable)
Resolution	1.7 to 17 meters in height
Transmitted power	upto 135W electrical or 15W acoustical
Antenna system	Paraboloid fiber glass dish (6ft. diameter) as reflector with transducer and horn fixed at its focus
Preamplifier sensitivity	10 nV rms or 0.1 microvolt
Preamplifier gain	110 db
Preamplifier bandwidth	Q 10
Receiver sensitivity	110 dBm
Bandwidth of filter	Q 100
Display	Facsimile recorder

placed at the focus of a 6-ft. diameter parabolic fiber glass dish. The backscattered signals are received by the same antenna and amplified through a remote preamplifier. The amplified signal, after proper filtration of the additional noise, is fed to the receiver. Finally, a 3-D facsimile is used to record the backscattered energy as a function of the height and time. The system is capable of probing the LPBL successfully up to a height range of 1 km. Other details about the system configuration are furnished in Table I [20].

The model has successfully recorded the lower atmospheric structures that appeared during premonsoon (March, April, and May), monsoon (June, July, and August), postmonsoon (September, October, and November), and winter (December, January, and February) seasons of this region. Though the system recorded various types of lower atmospheric structures, presently in this letter, we choose to concentrate on the six basic types of single layer structures (each representing a different thermodynamic state of the LPBL) that appeared at our site for

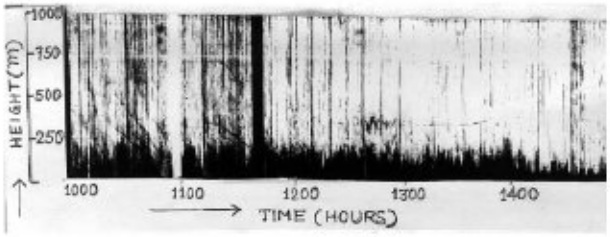

Fig. 2. Convective plumes.

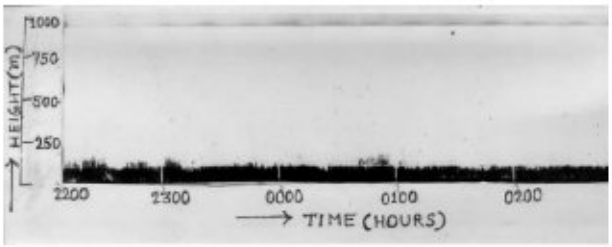

Fig. 3. Inversion with flat top.

more than 80% occasions during observations recorded over a complete year. The different categories used include convective plumes, inversion with flat top, inversion with small spikes, inversion with tall spikes, rising inversion, and rising inversion with convective plumes.

Fig. 2 describes the formation of typical convective boundary layer, recorded in February 1986. During the process of convection, warm air parcels go up from the ground (because of the low density), and cold air parcels from the upper level come down to fill up this place. The process repeats itself continuously during the period of convection. Identification of this convective activity from SODAR records is usually quite easy because thermal plumes organize themselves in a variety of sizes, both with height and time, as they pass through the SODAR antenna beam. This characteristic of the convective boundary layer with thermal plumes is categorized as class 1. It is seen to appear on cloudless, clear sunny days of all the four different seasons prevalent over this region. This class represents an unstable atmospheric condition. On the occurrence of this class, the transfer of heat, momentum, and energy from the surface level to the higher level and vice-versa takes place. That, in turn, tries to introduce in-mixing within the layer.

Fig. 3 describes the formation of the ground-based temperature inversion layer in the LPBL. Approximately a 150-m-thick surface-based layer was formed on the ground. This type of layer is generated on clear nights (associated with very light wind conditions) due to the emission of infrared radiations from the ground. On formation of this layer, the temperature lapse rate gets inverted, i.e., temperature increases with height. The SODAR observations describing the temperature inversion layer with flat top is categorized as class 2. During the daytime, solar radiations are the primary source to introduce turbulence into the lower atmospheric environment, whereas at night, in the absence of these solar radiations, wind is the main source of turbulence in LPBL. It is observed that this class is present during all the four seasons whenever the mechanical turbulence due to wind is negligible.

Under moderately high wind conditions, the temperature inversion layers formed are associated with small spikes, as seen

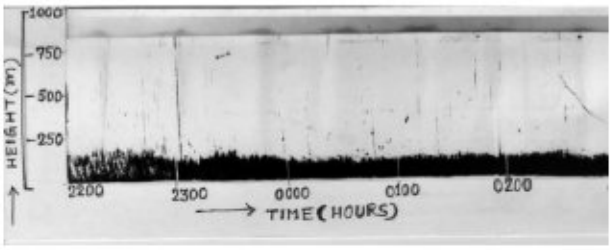

Fig. 4. Inversion with small spikes.

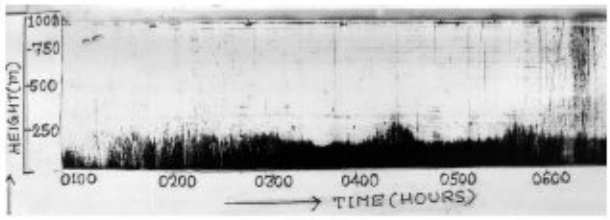

Fig. 5. Inversion with tall spikes.

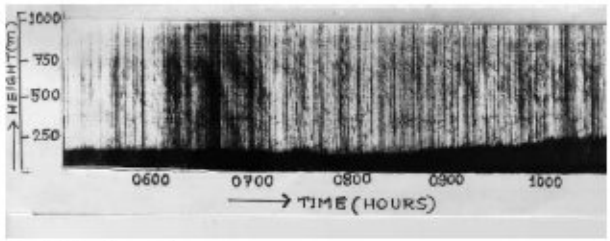

Fig. 6. Rising inversion.

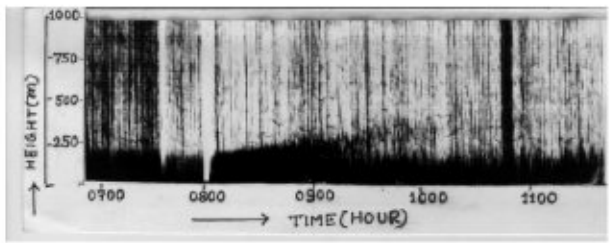

Fig. 7. Rising inversion with convective plumes.

on the top of the layer. These spikes are introduced due to small-scale mechanical turbulence caused by wind of moderate speed.

Fig. 4 shows the formation of a temperature inversion layer with small spikes and is categorized as class 3. Sometimes, under very high wind conditions, the temperature inversion layer may be associated with tall spikes, as observed in Fig. 5. This is categorized as class 4. Under this situation, the strong mechanical turbulence due to high wind speed tries to introduce an instability in the stable atmospheric structure (temperature inversion layer) formed during the night hours due to emission of infrared radiations from the earth surface.

In the early morning hours, SODAR records generally show ground-based temperature inversion layer. Turbulence is typically generated in this layer due to incoming solar radiations that try to erase the ground-based temperature inversion layer. Initially, just after sunrise, most of the solar energy is used in destroying the ground-based temperature inversion layer. With continuous solar heating, this layer rises higher, and after sometime, it becomes insensitive to SODAR detection. A SODAR-recorded rising inversion layer shown in Fig. 6 is categorized as class 5. This type of layer (class 5) appeared at

TABLE II
RECOGNITION SCORES (IN PERCENT) FOR SODAR DATA

Train	# nodes	6		8		10		12		15	
set. %	Classes	Train	Test	Train	Test	Train	Test	Train	Test	Train	Test
	1	92.86	61.97	92.86	64.79	85.71	67.61	92.86	66.20	85.71	69.01
	2	85.71	47.95	92.86	59.42	100.0	59.42	92.86	60.87	85.71	62.32
	3	92.86	35.56	100.0	37.21	92.86	61.90	100.0	58.73	100.0	60.32
20%	4	100.0	36.72	85.71	36.72	92.86	35.22	85.71	38.21	100.0	61.29
	5	92.86	55.36	92.86	58.93	100.0	60.71	100.0	62.50	100.0	64.29
	6	100.0	59.57	100.0	63.83	100.0	63.83	92.86	65.96	100.0	63.83
	Total	94.05	57.91	94.05	60.05	95.24	61.30	94.05	61.93	95.24	63.65
	Iteration	8032		8232		8820		8148		7950	
	r.m.s error	0.000064		0.000063		0.000059		0.000060		0.000058	
	1	95.24	69.01	90.48	73.24	95.24	74.65	100.0	73.24	95.24	76.06
	2	90.48	63.77	95.24	65.22	95.24	68.12	95.24	69.57	95.24	71.01
	3	100.0	61.90	95.24	60.32	95.24	60.32	100.0	61.90	95.24	60.32
30%	4	95.24	62.69	100.0	62.69	100.0	61.19	95.24	62.69	100.0	62.69
	5	95.24	62.50	95.24	64.29	100.0	66.07	95.24	69.64	100.0	69.64
	6	100.0	65.96	100.0	65.96	95.24	65.96	100.0	65.83	95.24	65.96
	Total	96.03	64.34	96.03	65.42	96.83	66.22	97.62	67.02	96.83	67.83
	Iteration	7686		7938		7434		7560		7686	
	r.m.s error	0.000061		0.000057		0.000058		0.000054		0.000055	
	1	92.86	73.24	96.43	74.65	92.86	76.06	96.43	74.65	100.0	73.24
	2	92.86	69.57	100.0	71.01	100.0	69.57	96.43	71.01	96.43	71.01
	3	96.43	60.32	92.86	63.49	96.43	66.67	96.43	65.08	96.43	68.25
40%	4	100.0	64.18	96.43	61.19	100.0	64.18	100.0	67.16	96.43	70.15
	5	100.0	73.21	96.43	76.79	96.43	73.21	100.0	71.43	100.0	71.43
	6	96.43	63.83	92.86	61.70	96.43	61.70	96.43	63.83	96.43	65.96
	Total	96.43	67.56	95.83	68.36	97.62	68.90	97.62	69.17	97.62	70.24
	Iteration	7032		7560		7392		7224		7056	
	r.m.s error	0.000058		0.000056		0.000053		0.000054		0.000052	
	1	94.29	71.83	97.14	73.24	100.0	74.65	97.14	74.65	97.14	76.06
	2	97.14	72.46	97.14	71.01	97.14	73.91	97.14	75.36	97.14	75.36
	3	100.0	65.49	97.14	65.08	97.14	66.67	100.0	69.84	100.0	73.02
50%	4	94.29	71.64	100.0	74.63	97.14	73.13	97.14	71.64	100.0	71.64
	5	100.0	73.21	100.0	71.43	100.0	71.43	100.0	73.21	100.0	73.21
	6	94.29	63.83	97.14	65.96	97.14	65.96	97.14	65.96	97.14	65.96
	Total	96.66	69.71	98.10	70.24	98.10	71.31	98.10	71.12	98.58	72.02
	Iteration	7770		7140		7560		7350		6720	
	r.m.s error	0.000056		0.000057		0.000055		0.000053		0.000051	

our site of observation throughout the year during cloudless, clear sunny days. This layer brings a drastic change in the thermodynamic state of the LPBL. During night hours, due to the formation of the temperature inversion layer, a stable structure persist in the LPBL that traps all the pollutants within its height. Due to formation of rising temperature inversion layer (class 5), a transition of atmosphere from a stable state to an unstable state takes place, and the pollutants that were trapped inside the stable layer get dispersed and diffuse in the higher level with the rise of this layer. As a result, the pollution density in the LPBL reduces and finally becomes least with the disappearance of this layer.

Fig. 7 depicts the rising inversion layer capping a convective boundary layer and is probably the most recognizable atmospheric feature on the SODAR record. This type of mixed layer is categorized as class 6. Under this situation, the formation of thermal plumes signifies that the transition of the lower atmosphere from stable to unstable state is completed, and the transfer of heat, momentum, and energy may take place freely from the earth's surface to the higher level and vice-versa.

III. IMPLEMENTATION AND RESULTS

SODAR observations are typically recorded on electrosensitive chart papers. The width of the paper describes the height scale (the vertical length of the atmosphere probed by the SODAR, i.e., 1 km for the system described here), whereas the length of the paper denotes the time scale. The numerical value of the average height of the backscattered sound energy at a particular instant can be obtained from the chart paper.

We selected 3-h duration of data from each of the categories described in Section II. This observation was digitized to get the numerical value of average height of backscattered sound energy at intervals of 2 min. In this manner, 90 data points were obtained from the charts for each category. These were used as the input features. The six SODAR pattern categories correspond to the output classes and are available at http://www.isical.ac.in/~sushmita.

A three-layered MLP, with standard backpropagation learning, was used for classifying the patterns. Random sets of 30 sequential observations, from the total 90 data points in each pattern category, constituted a training pattern with 30 attributes (input nodes) for that class. Six nodes were involved at the output layer. Various three-layered networks were used with different numbers of hidden nodes (6, 8, 10, 12, 15) and training sets (20%, 30%, 40%, 50%). On further increasing the number of hidden nodes (say, 20 or 25), the performance remained unchanged. The training set size $x\%$ refers to random classwise selection of $x\%$ training data (a sequence of 30 points in the chart) from the entire dataset. The remaining $(100-x)\%$ data constitute the test set in each case.

Table II shows that an increase in training set size leads to better performance over the training and testing sets for all SODAR pattern categories. A hidden layer with larger number of hidden nodes yields better generalization over the test set.

IV. Conclusion and Discussion

The LPBL plays an important role in the transfer of heat, momentum, and energy from the lower level to the higher level and vice-versa. It is responsible for the formation of different types of storms and various other mesoscale and microscale atmospheric phenomena such as fog, haze, hail, rain, and convection and different types of temperature inversion layers. Therefore, a need to probe the LPBL on a regular basis has long been realized by meteorologists, scientists, and engineers all over the world. The SODAR system has emerged as a useful technique that provides information about the formation of different types of temperature inversion layers, thermal plumes, fog layer, elevated temperature inversion layers, and various other type of lower atmospheric structures, at a low cost and on a continuous basis. However, a lack of some standard computer-based technique for the identification of the different types of useful SODAR patterns has resulted in the data being used on a very limited basis.

The use of the MLP for identifying the different types of SODAR patterns is expected to overcome the above problems. Neural network models are inherently suitable in data-rich environments and can extract underlying relationships from the data domain. This reduces dependence on the human expert for the identification process.

This being one of the first approaches in classifying SODAR data, which is inherently extremely noisy (as evident from Figs. 2–7), it was very difficult to get good classification on the raw dataset. This is observable from Table II. The generalization over the test set was not that good. But given this data and the fact that this is one of the first studies in a new direction, some flaws are bound to remain. This letter serves as the stepping stone toward further refined study in this direction.

We have plans to introduce some forms of feature extraction in the next phase of our work. That would definitely provide better generalization over the test set. We are also investigating the extension of this model to handle multilayered SODAR structures and other useful events, in order to exploit the full potential of the SODAR data. Finally, this holds promise for researchers working in the domains of atmospheric sciences, remote sensing, microwave propagation, civil aviation, air pollution, and meteorology.

Acknowledgment

The authors acknowledge D. Mukhopadhyay for his programming support.

References

[1] P. S. Arya and R. Holton, *Introduction to Micrometeorology*. San Diego, CA: Academic, 2001.
[2] R. B. Stull, *An Introduction to Boundary Layer Meteorology*. Dordrecht, The Netherlands: Kluwer, 1988.
[3] H. J. Crictchfield, *General Climatology*. Englewood Cliffs, NJ: Prentice-Hll, 1960.
[4] E. C. Barrett and L. F. Cutis, *Introduction to Environmental Remote Sensing*. London, U.K.: Chapman and Hall, 1982.
[5] R. G. Reeves and F. J. Janza, *Manual of Remote Sensing: Theory Instruments and Techniques*. Falls Church, VA: Amer. Soc. Photogramm., 1975, vol. 1.
[6] G. W. Gilman, H. B. Coxhead, and F. H. Wills, "Reflection of sound signals in the troposphere," *J. Acoust. Soc. Amer.*, vol. 18, pp. 274–283, 1946.
[7] L. G. Mcallister, J. R. Pollard, A. R. Mahohey, and P. J. R. Shaw, "A new approach to the study of atmospheric structure," *Proc. IEEE*, vol. 57, pp. 579–587, 1969.
[8] C. G. Little, "Acoustic methods for the remote probing of the lower atmosphere," *Proc. IEEE*, vol. 57, pp. 571–578, 1969.
[9] S. P. Singal, "Acoustic sounding studies of the atmospheric boundary layer," Meteorol. Service, Wellington, New Zealand, Tech. Rep. 30, 1988.
[10] V. Rapoport, N. Mityakov, V. Zinichev, and Y. Sazonov, "The study of atmospheric turbulence with an acoustic locator," *IEEE Trans. Geosci. Remote Sensing*, vol. 40, pp. 247–250, Feb. 2002.
[11] K. S. Ravi, S. V. B. Rao, M. J. Kesava Murthy, H. N. Dutta, S. K. Sarkar, and B. M. Reddy, "A study of tropospheric scintillations using SODAR," *Proc. Inst. Elect. Eng. H*, vol. 1.38, pp. 313–318, 1991.
[12] S. Haykin, *Neural Networks: A Comprehensive Foundation*. New York: Macmillan, 1994.
[13] J. M. Zurada, *Introduction to Artificial Neural Systems*. New York: West, 1992.
[14] J. T. Tou and R. C. Gonzalez, *Pattern Recognition Principles*. London, U.K.: Addison-Wesley, 1974.
[15] A. Pal, S. Choudhury, N. C. Deb, and M. Dey, "Some Pattern recognition issues in acoustic sounding," Applied Statist. Div., Indian Statist. Inst., Kolkata, India, Tech. Rep. ASD/2002/1, 2002.
[16] A. Mukherjee, P. Pal, and J. Das, "Classification of SODAR data using fractal features," in *Proc. 3rd Indian Conf. Computer Vision, Graphics and Image Processing*, 2002, pp. 203–207.
[17] C. Marzban and G. J. Stumpf, "A neural network for tornado prediction based on doppler radar-derived attributes," *J. Appl. Meteorol.*, vol. 35, pp. 617–626, 1996.
[18] ——, "A neural network for damaging wind prediction," *Weather Forecasting*, vol. 13, pp. 151–163, 1998.
[19] S. Choudhury, S. Mitra, and S. K. Pal, "Neuro-fuzzy classification and rule generation of modes of radiowave propagation," *IEEE Trans. Antennas Propagat.*, vol. 51, pp. 862–871, Apr. 2003.
[20] S. Choudhury, "Tropospheric VHF propagation studies using ground-based in-situ and acoustic remote sensing technique," Ph.D. thesis, Univ. Calcutta, Calcutta, India, 2000.